NASA TECHNICAL MEMORANDUM

NASA TM X-71793

NASA TM X-71793

(NASA-TM-X-71793) FLAT-PLATE SOLAR-COLLECTOR PERFORMANCE EVALUATION WITH A SOLAR SIMULATOR AS A BASIS FOR COLLECTOR SELECTION AND PERFORMANCE PREDICTION (NASA) 52 p HC $4.25 CSCL 10B G3/44

N75-32591

Unclas 41104

FLAT-PLATE SOLAR-COLLECTOR PERFORMANCE EVALUATION WITH A SOLAR SIMULATOR AS A BASIS FOR COLLECTOR SELECTION AND PERFORMANCE PREDICTION

by Frederick F. Simon
Lewis Research Center
Cleveland, Ohio 44135

TECHNICAL PAPER presented at the
1975 International Solar Energy Society Meeting
Los Angeles, California, July 28 - August 8, 1975

FLAT-PLATE SOLAR-COLLECTOR PERFORMANCE EVALUATION WITH A SOLAR SIMULATOR AS A BASIS FOR COLLECTOR SELECTION AND PERFORMANCE PREDICTION

by Frederick F. Simon

National Aeronautics and Space Administration
Lewis Research Center
Cleveland, Ohio

E-8470

ABSTRACT

The use of a solar simulator for performance determination permits collector testing under standard conditions of wind, ambient temperature, flow rate and "Sun." The performance results determined with the simulator have been found to be in good agreement with outdoor performance results.

This paper reports the measured thermal efficiency and evaluation of 23 collectors which differ according to absorber material (copper, aluminum, steel), absorber coating (nonselective black paint, selective copper oxide, selective black nickel, selective black chrome), type of glazing material (glass, Tedlar, Lexan, anti-reflection glass), the use of honeycomb material and the use of vacuum to prevent thermal convection losses. The collectors are given performance rankings based on noon-hour solar conditions and all-day solar conditions. The determination with the simulator of an all-day collector performance is made possible by tests at different incident angles. The solar performance rankings are made based on whether the collector is to be used for pool heating, hot water, absorption air conditioning, heating, or for a solar Rankine machine.

Another test which aids in selecting collectors is a collector heat capacity test. This test permits a ranking of collectors according to their heat capacity (and time constant), which is a measure of the rapidity of a collector's response to transient solar conditions. Results are presented for such tests.

Final considerations for collector selection would of course be made on the basis of cost and the reliability of performance over the required life of a collector. Results of a cost-effectiveness study is given for conditions corresponding to those required for absorption a/c or heating. These results indicate that the additional cost involved in the upgrading of collector performance (selective surfaces, anti-reflection glass, etc.) appears to be cost effective and therefore justified. Some data are also presented to illustrate a method for the determination of outdoor performance degradation by use of simulator tests carried out before and after a period of outdoor operation.

INTRODUCTION

An area presently being investigated by the NASA-LeRC in its efforts to aid in the utilization of alternate energy sources, is the use of solar energy for the heating and cooling of buildings. An important part of the solar heating and cooling effort at the Lewis Research Center is the investigation of flat-plate collectors which have the potential to be efficient, economical, and reliable. Efficient collectors will be an important consideration in the realization of effective solar cooling systems.

The approach being taken to determine collector performance is to test collectors under both simulated (indoor) and actual (outdoor) conditions.

The rationale for the use of a solar simulator was given in reference 1. Basically, the use of a simulator in the indoor testing of collectors allows for a standard condition of solar radiation, ambient temperature, flow rate, and wind speed. With such "standard" test conditions, it becomes possible to compare the performance of different collectors, or the effect on performance of a design variation on a given collector. Validation of collector performance obtained under indoor simulated conditions is made possible by outdoor collector tests performed at the Lewis Research Center (ref. 2).

This paper presents the experimental performance of 23 collectors by use of a solar simulator. Selected tests were performed on collectors placed outdoors for a comparison with the indoor tests. Data are also

shown to demonstrate the utility of using the solar simulator to determine collector heat capacity and to determine collector degradation after extended outdoor testing. The significance of experimentally determined collector performance parameters is discussed. Finally, the performance results from the solar simulator are used to show how such results can be used, along with cost data, to determine the relative cost effectiveness of several different collectors.

COLLECTORS TESTED

A list of collectors tested and some of their characteristics is given in Table I. The collectors listed differ according to absorber material (copper, aluminum, steel), absorber coating (nonselective black paint, selective copper oxide, selective black nickel, selective black chrome, selective chemical-etched aluminum) type of transparent cover material (glass, Tedlar, anti-reflection glass), the use of honeycomb material and the use of vacuum to prevent thermal convection losses. The performance results for collectors 1 - 16 were previously reported (refs. 5 to 9). The performance of collector number 22 was determined on contract to Honeywell by using a duplicate of the simulator used at the Lewis Research Center (ref. 3).

Table I displays four different collector areas; namely, the total area (A_T), the transparent cover area (A_g), the absorber area (A_a) and the effective area (A_e). The effective area is the area that actually receives the sun's energy. In those cases where collectors do not have obstructions to the solar radiation, the effective area is equal to the absorber area. The parameters a_θ, b_θ, c_θ and b_o will be discussed subsequently in the results and discussions.

EXPERIMENTAL METHOD

Experimental Facility

A drawing of the facility is presented in figure 1. The primary components of the facility are the energy source (solar simulator), the

liquid flow loop, and the instrumentation and data acquisition equipment. A summary of information describing the facility is presented in Table II.

Solar Simulator

The solar simulator has been designed for nearly collimated radiation with a spectral output close to that of air-mass 2 sunshine (ref. 4). This has been accomplished at a reasonable cost due to the use of commercially available tungsten halogen lamps that use dichroic reflectors for rejection of infrared radiation. A photograph of the simulator is shown in figure 2. The simulator shown in figure 2 consists of 143 tungsten halogen 300 watt lamps placed in a modular array with Fresnel lenses placed at the focal distance so as to collimate the radiation. The spectral match of this simulator with actual sunshine is of special importance in the testing of selective surfaces. A comparison of spectral characteristics of the simulator output with air-mass 2 sunlight is given in Table III. Table III demonstrates that the solar simulator does an excellent job of simulating the sun's radiation.

A more definitive test of the simulator's ability is a comparison of the results of collectors tested with the simulator and tested outdoors. A test of this type was performed as part of a contract to the Honeywell Corporation in Minneapolis, Minnesota (ref. 3). A selective (black nickel) two-glass and a nonselective (black paint) two-glass collector were tested both indoors under simulated conditions and outdoors. The solar simulator used by Honeywell is a duplicate of the NASA-Lewis solar simulator. A comparison of indoor and outdoor tests is given in figures 3a to 3d. The time prior to reaching 180° F (denoted by arrow) shown in figures 3a to 3d was a period in which the collector and the rest of the system was warming up. Figures 3a to 3d indicate that the solar simulator does a good job of predicting the performance of collectors tested outdoors.

In these comparison tests, the time required for the collectors to respond to a change in solar radiation was sufficiently small (approximately 10 min.) so that the steady-state prediction of the simulator did a good job of following the outdoor transients (figs. 3c and 3d).

Coolant Flow Loop

The flow loop consists of storage and expansion tanks, pump, heater, test collector, and the required piping shown schematically in figure 4. The hot fluid storage tank is a commercially available water heater for home use. The tank has two electrical immersion heaters, 5 kilowatts each, and has a capacity of 80 gallons. The pump is a gear type unit driven by a 1/4 horsepower electric motor through a variable speed drive.

A heat exchanger using city water as a coolant is used to control the temperature of the collector coolant fluid at the collector inlet.

A 50/50 by weight mixture of ethylene-glycol and water is used in the liquid loop. The specific gravity of the mixture is checked with a precision grade hydrometer. To suppress vapor formation the entire flow loop is pressurized to approximately 15 psig by applying a regulated inert gas pressure to the top of the expansion tank.

Instrumentation and Data Acquisition

The parameters needed to evaluate collector performance are: liquid flow rate, liquid inlet and outlet temperatures, the simulated solar flux, wind speed, and the ambient temperature. The flow rate is determined with a calibrated turbine-type flow meter that has an accuracy better than one percent of the maximum flow. The collector inlet and outlet temperatures are measured with ISA type E thermocouples (chromel-constantan). The thermocouples were calibrated at 32° and 212° F. The error in absolute temperature measurement is less than 1° F and the differential temperature error between the inlet and outlet thermocouples is less than 0.2° F.

The ambient temperature is measured with an ISA type E thermocouple mounted in a radiation shield. The simulated solar flux is measured with a water-cooled Gardon type radiometer having a sapphire window. The radiometer was calibrated with a National Bureau of Standards irradiance standard.

In addition to the measurements of the basic parameters mentioned above, the following parameters are also measured for the purpose of obtaining detail information.

1. Collector absorber plate temperatures } (for a selected few col-
2. Collector glass temperatures } lectors)
3. Collector coolant pressure and pressure drop
4. Temperature of surroundings

The millivolt-level electrical outputs of the measuring instruments are recorded on magnetic tape by the use of a high speed data acquisition system. The information from the tape is sent to a digital computer for data reduction and computation. The computer results are printed out in the test facility within minutes after the data is initially recorded.

Test Procedure

The collectors are mounted on the test stand and positioned so that the radiant flux is normal to or at different angles to the collector. Variation of the incident angle is accomplished by rotating the test stand about the vertical axis. The present tests were run at a tilt angle of 57 degrees. The flow rate is adjusted to a value corresponding to 10 pounds per hour per square foot of collector absorber area. Before the simulator is turned on, the collectors are given time to achieve thermal equilibrium at the inlet temperature chosen (1 hr or more). After thermal equilibrium is established for a given inlet temperature, the simulator is turned on and the desired radiant flux is obtained by adjusting the lamp voltage. After steady-state conditions occurred, usually in 10 to 15 minutes, data is recorded. The radiant flux is then readjusted to a second value at the same collector inlet temperature, steady-state conditions obtained, and data again recorded. The collector inlet temperature is then set to another value, and the procedure repeated.

To determine collector heat capacity, the simulator is turned off and a record is made of the outlet fluid temperature versus time for an inlet temperature equal to the ambient temperature.

COLLECTOR TEST RESULTS

The experimental efficiency of each collector was calculated using the following equation:

$$\eta = G C_p (T_0 - T_1)/q_{dr} \tag{1}$$

Where G is defined as the flow rate per unit of effective area for solar collection

$$G = w/A_e \tag{2}$$

Collector efficiencies were determined for an average flow rate of 10 lb/hr ft^2, inlet temperatures ranging between 75^o to 210^o F, a simulated heat flux ranging between 150 to 350 Btu/hr ft^2, wind speed of 7 mph and an ambient temperature which averaged 80^o F.

Correlative method. - Justification for the method of correlating collector test data was presented in reference 1. Basically the method involves the utilization of the analytical equations that describe collector performance. The three equations useful for correlating collector performance are as follows:

$$\eta = \alpha\tau - \left[\left(\frac{A_a}{A_e}\right) U_L (\bar{T}_p - T_a)\right] \Big/ q_{dr} \tag{3}$$

$$\eta = F' \left\{ \alpha\tau - \left[\left(\frac{A_a}{A_e}\right) U_L (\bar{T}_f - T_a)\right] \Big/ q_{dr} \right\} \tag{4}$$

$$\eta = F_R \left\{ \alpha\tau - \left[\left(\frac{A_a}{A_e}\right) U_L (T_1 - T_a)\right] \Big/ q_{dr} \right\} \tag{5}$$

Table I indicates that for many collectors the radiant energy reaches the absorber plate unobstructed so that the effective area for solar collection (A_e) is equal to the absorber area ($A_e = A_a$). For these cases the area ratio shown in equations (3), (4), and (5) is unity ($A_a/A_e = 1$). While the efficiency has been calculated based on an effective area so as to permit a collector heat balance that results in equations (3), (4), and (5),

it is possible from the data of Table I to calculate efficiency based on the maximum collector area (A_T), absorber area (A_a) and the transparent cover area (A_g): i.e.

$$\eta, A_T = \eta, \text{Eq } 1 \times A_e/A_T \tag{6a}$$

$$\eta, A_a = \eta, \text{Eq } 1 \times A_e/A_a \tag{6b}$$

$$\eta, A_g = \eta, \text{Eq } 1 \times A_e/A_g \tag{6c}$$

Examples of how equations (3), (4), and (5) are used in correlating data and obtaining collector parameters ($\alpha\tau$, F', F_R, U_L) were given in references 1, 6, and 7.

Performance curves of a black nickel two-glass collector (number 5, Table I) from reference 6 are shown in figures 5(a) to (c). Fron an inspection of equations (3) to (5) it can be seen that by plotting efficiency against temperature difference divided by radiant flux (η against $(T - T_a)/q$) as indicated in figure 5, it is possible to obtain key collector parameters from the slope and intercept of the correlating lines. As explained in reference 1, the values of $\alpha\tau$, U_L, F', and F_R obtained in the above manner will give specific information on why a collector excelled or why it performed poorly. The use of this correlation approach has an additional advantage in the case where the effective collector area was greater than the area of radiation provided by the solar simulator ($A_e > 16$ ft^2). This situation was encountered in four collectors (numbers 14, 17, 19, and 23). In these cases a reflecting shield was placed above a portion of the collector to create a section of the collector which received a uniform supply of energy from the simulator, thus making the effective area equal to approximately the simulator maximum area (16 ft^2). The effect of the shield is to increase the slope of the correlating equation as indicated by the following equation:

$$\eta' = F_R \left\{ \alpha\tau - \left[\left(\frac{A_a}{A'_e} \right) U_L (T_1 - T_a) \right] \Big/ q_{dr} \right\} \qquad (7)$$

The reflecting shield was maintained at an ambient temperature conditions at a distance of 2 inches from the collector. This allowed for the sink temperature for collector heat loss to be the same for all portions of the collector and thereby maintain the same heat loss coefficient that the collector would have without the reflecting shield. Because of this the correlation equation for performance with the shield can be modified to obtain the performance equation for the normal case when the entire collector receives radiant energy. Equation (7) is modified as follows:

$$\eta = F_R \left\{ \alpha\tau - \left[\left(\frac{A'_e}{A_e} \right) U_L (T_1 - T_a) \right] \Big/ q_{dr} \right\} \qquad (8)$$

Equation (8) indicates that the collector data obtained by use of a shield can be modified by multiplying the slopes of the correlating lines (of the type shown in fig. 5) by the ratio of the effective collector area with and without the shield (A'_e/A_e).

Collector efficiency curves for zero incident angle. - The collector efficiency curves for zero incidence angle are shown in figures 6 through 10 in terms of the inlet temperature, the ambient temperature and the radiant flux level.* The results shown in figures 6 to 10 illustrates the large performance differences that exist among the collectors tested. In general no one collector design can maintain the highest efficiency throughout the entire range of the abscissa. This is due to considerations which determine collector performance; considerations that are not always compatible. One consideration is the slope of the curves which is a measure of the heat loss. Collectors 8 and 9 (fig. 8) and 10 and 11 (fig. 9) differ by the presence of a mylar honeycomb between the absorber plate and the transparent cover. The effect of the honeycomb material is to reduce

*Use of the inlet temperature allows for a convenient basis in collector performance calculations.

convection and radiation losses, resulting in a reduced slope for the performance curves. Another consideration effecting heat loss is coating absorptance (α) and cover transmittance (τ). Collectors with two covers while decreasing heat loss also lower the cover transmittance as compared to single cover collectors. For comparable absorptance values, the product of $\alpha\tau$ is lower for the two-cover collector compared to the single covered ones. This results in the two-cover collector having lower values of the performance curve intercept and higher efficiencies at higher values of the abscissa due to lower heat losses. The single-covered collectors are higher performers at lower inlet temperatures, but a crossover point is reached whereby at higher abscissa values the double-covered collectors become better performers. This effect is demonstrated in figure 10 by comparing collectors 1 and 8, and occurs for collectors 9 and 10 and 8 and 11. In addition to reducing heat loss by the use of honeycomb and/or an additional transparent cover, use is also made of vacuum (collector 16) and selective surfaces (collectors 2, 3, 4, 5, 6, 7, 15, 16, 17, 19, 20, 21 and 22). The combination of vacuum and a selective surface has a dramatic effect on the heat loss as indicated by the experimental slope of collector 16 (figs. 6 and 10). The effect of using low emittance coatings such as black nickel and black chrome can be seen in figure 10 where a comparison may be made between a selective black nickel 2-glass collector (5) and a nonselective black paint 2-glass collector (1). The reduction of thermal radiation losses by the use of selective coatings is clearly an advantage for the case of low flux conditions and/or high temperature.

The intercept of the performance curves of figures 6 to 10 is governed as indicated in equation (5) by the absorptance, the transmittance and the flow factor. In figure 8 where the performance curves for nonselective one cover collectors are given, the intercept for collector 18 is lowest due to the effects of low cover transmittance, and poor collector plate heat transfer to the fluid carrying tubes. The poor collector plate heat transfer due to having tubes clamped to the collector plate rather than soldered produces a lower than desired value of the flow factor (F_R).

The effect of absorptance on the intercept of the correlating curve is dramatized by comparison of collector 5 and collector 7 (fig. 7). While

both the collectors had a black nickel coating, the absorptance of collector 5 was 0.95 and the absorptance of collector 7 was 0.73 (Table I).

A method of increasing the level of collector performance is to use anti-reflecting glass to increase the amount of transmitted solar energy. This is demonstrated in figure 7 by the test results for a black nickel coated collector with anti-reflection glass (22). By comparing this collector (22) with the same type and design without anti-reflection glass (5) it can be seen the effect of the anti-reflection glass is to increase the level of performance (higher intercept value) without much effect on the collector heat loss (slope of correlating lines).

The summary figure (fig. 10) shows that by increasing the amount of solar radiation through the cover system (anti-reflection glass) and decreasing the radiation loss (black nickel selective surface) a high performance collector is possible. A high performing collector may also be achieved for conditions of high temperature and/or low radiant flux by the use of a selective surface and vacuum (collector 16).

Incident angle modifier. - To account for the effect of temperature on the heat loss coefficient (U_L), the correlating curves of figures 6 to 10 may be expressed in the following manner:

$$\eta = a_\theta - (b_\theta \theta + c_\theta \theta^2) \tag{9}$$

where

$$\theta = (T_1 - T_a)/q_{dr}$$

and the experimentally determined values of a_θ, b_θ and c_θ are listed in Table I.

The intercepts (a_θ) of figures 6 to 10 are a function of incident angle. This may be seen in equations (5) and (9) for $\theta = o$, since the absorptance and transmittance are functions of the incident angle.

Experimental results obtained with the simulator indicate, as expected, that different incident angles affect only the intercept of the correlating curve (fig. 11). The angular dependence of the intercept valve (a_θ) may

therefore be determined by a determination of collector performance at different incident angles at an inlet temperature equal to the ambient temperature ($\theta = 0$). The intercept value may be nondimensionlized as follows:

$$K_{\alpha\tau} = \frac{\eta_{\theta_i, T_1=T_a}}{\eta_{\theta_{i=0}, T_1=T_a}} = \frac{a_{\theta, \theta_i}}{a_\theta} \tag{10}$$

This permits equation (9) to be expressed in terms of the incident angle effect as follows:

$$\eta = K_{\alpha\tau} a_\theta - (b_\theta \theta + c_\theta \theta^2) \tag{11}$$

Equation (11) represents the complete correlation curve obtained by use of the solar simulator approach.

An example of the experimentally determined modifier is shown in figure 12. It can be seen that use of the correlating approach indicated by figure 12 requires many experimental values. A better approach is to use the linear correlation suggested by Souka and Safwat (ref. 10) and further demonstrated by Simon and Buyco (ref. 11). Figure 12 is replotted in figure 13 in terms of a linear correlating parameter. The correlating lines of figure 13 may be expressed as

$$K_{\alpha\tau} = 1.0 + b_o \left(\frac{1}{\cos \theta_i} - 1.0 \right) \tag{12}$$

The value of the constant (b_o) is a function of the collector design and is larger for increased transmission or reflection losses such as occurs with an increased number of collector covers or the use of honeycomb material (fig. 14).

In reference 8 it was experimentally shown that the angular response of a tubular-glass collector (number 16, Table I) differed from that of a traditional collector. The design of the tubular-glass collector is such

that its efficiency increases with an increase in the incident angle. This effect results in a positive slope for the linear correlation of the incident angle modifier (fig. 14). Experimentally determined values of the constant (b_o) are given in Table I. As shown in reference 11, equation (12) may be employed for a determination of the product of absorptance and transmittance for diffuse radiation ($\overline{\alpha\tau}$). The result given in reference 11 is

$$\overline{\alpha\tau} = (\alpha\tau)_{\theta_i=0}\,(1 + b_o) \tag{13}$$

If we attempt to obtain a correlation curve for solar radiation consisting of both direct and diffuse energy, we find that the value of the intercept ($a_{\theta,x}$) is a function of the diffuse and direct component. From reference 12 an analytical equation may be obtained

$$a_{\theta,x} = (a_\theta + \bar{a}_\theta x)/(1 + x) \tag{14}$$

where

$$x = q_{df}/q_{dr}$$

Use of equation (13) results in

$$a_{\theta,x}/a_\theta = [1 + (1 + b_o)x]/(1 + x) \tag{15}$$

Values of the correlation intercept for both total direct (a_θ) and partial diffuse ($a_{\theta,x=0.77}$) were obtained in reference 3 by use of a glass light diffuser between the collector and the simulator. The experimental value of the intercept ratio ($a_{\theta,x=0.77}/a_\theta$) determined was 0.96. Use of equation (15) gives a value of this ratio of 0.93. The comparison of the experimental and calculated ratios appears to justify the use of equation (15).

Collector performance parameters. - Collector performance parameters of eleven collectors based on the correlations according to equations (3) to (5) are shown in Table IV. These collector parameters permit a determination of the "why" a collector performed the way it did. Collectors 5 and 11 are basically the same with exception of the coating used on the absorber plate. This basic sameness in construction is reflected in nearly the same values of F' and F_R and in nearly equal values of $\alpha\tau$. Since the absorptance for the two collectors is identical, their difference in performance is attributable to the black nickel-coated collector (5) having a lower experimental heat loss coefficient (U_L) than that of the black paint-coated collector (11). Comparing collector number 5 with collector number 7, it can be seen that the greatest single factor contributing to the latter's lower performance was the lower value of absorptance. The effect that a honeycomb has on reducing convection and radiation heat loss becomes clear from a comparison of collectors 10 and 11. The performance test on collector 10 was performed by placing mylar honeycomb material in collector 11; therefore, a direct comparison for heat loss effect may be made. As Table IV shows the heat loss coefficient went from a value of 0.80 to value of 0.57 by using honeycomb. This heat loss value is essentially the same as that obtained with a black nickel absorber plate (collector 5) in the same type of collector box as collector 10. Therefore this particular honeycomb plus a nonselective surface was equivalent to a black nickel selective surface.

The effect of increased heat loss is to lower the value of the flow factor (F_R) as is shown in Table IV for collector 14. This lowering of the flow factor has the effect of decreasing the intercept of the correlating curve as shown in figure 8. The high heat loss of collector 14 was due to large back and edge losses. When these losses are minimized, a decrease in the overall heat loss can be achieved as can be seen by comparing collector 14 with collector 1.

Comparison of the heat loss coefficient for a selectively coated nonevacuated collector (5) with a selectively evacuated collector (16) demonstrates the value of a vacuum in reducing or eliminating convection heat loss. Also shown in Table IV are some of the theoretical values of the heat loss coefficient. It can be seen that the experimental values of heat

loss coefficient are larger than the analytical prediction. In the case of collectors 5 and 11, references 3 and 11 demonstrated that this difference was due to higher internal convection heat losses than determined from standard natural convection heat loss correlations.

Collector heat capacity. - The test procedure of recording the outlet temperature after the simulator lamps are turned off, for an inlet temperature equal to the ambient temperature, permits use of the following equation for collector heat capacity derived in Appendix A.

$$C_c = \frac{\left(F'U_L + \frac{GC_p}{K}\right)(t_2 - t_1)}{\ln\left[\frac{T_0(t_1) - T_a}{T_0(t_2) - T_a}\right]} \tag{16}$$

where

$$K = \frac{GC_p}{F'U_L}\left(\frac{F'}{F_R} - 1\right)$$

Experimental values of the collector heat capacity calculated by use of equation (16) are shown in Table V. Also shown in Table V are estimated results from reference 13. There is general agreement between the experimental and estimated results of collector heat capacity. The collector heat capacity is an important measure of the transient properties of the collector, such as the collector warm-up time and the time required to react to changes in the solar flux. The lower the collector heat capacity, the shorter time required for collector warm-up and response to a changing flux. Increasing the number of collector components (glass, honeycomb, insulation, etc.) should increase the collector heat capacity. This is demonstrated by collectors 8, 10 and 11 where the same collector design shows an increased heat capacity from the baseline (8) as another glass cover is added (11) and finally as a mylar honeycomb material is added (10). Use of increased insulation also increases the capacity (number 17

has about one inch more of insulation than number 14). The larger than normal heat capacity of the evacuated tubular collector (number 16) is due to a large amount of liquid heat transfer fluid within the collector.

The values of the heat capacity given in Table V can be used to calculate a collector time constant, i.e., the time required for the collector efficiency to reach 99 percent of the equilibrium value after the collector is subjected to a step rise in heat flux (such as occurs after a cloud passes). The time constant for this case may be calculated from the equation derived in Appendix B.

$$t_c = \left(\frac{C_c}{F'U_L + \frac{GC_p}{K}} \right) \times \ln 100 \qquad (17)$$

A listing of time constants calculated by using equation (17) is also shown in Table V. Table V shows that most collectors have a time constant of approximately 10 min, i.e., it requires 10 minutes for these collectors to reach a new equilibrium condition after there has been a change in the solar flux. As explained in reference 13 the performance of such collectors may be predicted without the consideration of transient effects. However, this would not be the case for a collector such as number 16 which has a large time constant.

Depending upon the dynamics of solar heating and cooling systems, the need for collector heat capacity may be of some importance. Such a need will clearly be more important for collectors of high heat capacity because of their high time constants. A table of collector capacity values such as Table V will aid in selecting collectors when system dynamic considerations are important. However, a more important consideration for collector selection is its efficiency for energy collection, and, of course, its cost.

COLLECTOR PERFORMANCE RANKING

In reference 11 it was demonstrated how performance values obtained

with a simulator may be used for "real-life" collector performance prediction. Collector performance curves such as given in figure 5 were used in reference 7 for collector performance ranking. Reference 7 made collector performance calculations based on one value of the solar flux and pointed out the need for making solar comparison based on an all-day basis. This may be done by the use of a standard clear summer day (fig. 15), a standard clear winter day (fig. 16) a standard cloudy winter day (fig. 17) and the following equation from reference 11.

$$\eta = K_{FR}\left\{a_{\theta}[K_{\alpha\tau}K_{dr} + K_{df}(1 + b_o)] - K_{U_L}(b_{\theta}\,\theta + c_{\theta}\,\theta^2)\right\} \quad (18)$$

Where the coefficients a_{θ}, b_{θ}, c_{θ}, and b_o are obtained from the correlation of the simulator data as previously explained and are given in Table I for the collectors of this report. For the purpose of collector performance comparison, the flow rate per unit of collector area is the same as that used in the simulator testing (10 lb/hr ft^2, $K_{FR} = 1.0$). The tilt angle for summer solar data is 19 degrees and the winter solar data is 65 degrees. Using the same wind condition as experienced by the collectors in the simulator facility means that the only modifications needed to be made in equation (18) are for tilt angle and ambient temperature. The following are the conditions and equations used for the collector performance calculations for the different functions a collector may be required to perform:

A. Summer conditions (fig. 15)

1. Heating of swimming pools
   $T_1 = 86^{\circ}$ F
2. Hot water
   $T_1 = 140^{\circ}$ F
3. Solar a/c
   $T_1 = 200^{\circ}$ F
4. Solar Rankine
   $T_1 = 240^{\circ}$ F

$$\eta = a_{\theta}[K_{\alpha\tau}K_{dr} + K_{df}(1 + b_o)] - 1.06\,(b_{\theta}\,\theta + c_{\theta}\,\theta^2) \quad (19)$$

B. Winter conditions (figs. 16 and 17)

1. Heating

$T_1 = 120^{o}$ F

$$\eta = a_\theta[K_{\alpha\tau}K_{dr} + K_{df}(1 + b_o)] - K_{U_L}(b_\theta\,\theta + c_\theta\,\theta^2) \qquad (20)$$

$K_{U_L} = 1.0$ non-selective surfaces

$K_{U_L} = 1.1$ selective surfaces

The fact that selective surfaces appear to be more sensitive to ambient temperature and sky temperature changes for low inlet fluid temperatures was demonstrated in reference 11 (fig. 18). Some experimental justification of this effect is seen in some recent results (ref. 14).

The resulting calculations permit us to rank collectors according to efficiency for a noon hour and an all-day basis as is shown in Table VI(a) and (b).

Table VI(a) and (b) shows, as expected, that in the case of pool heating a simple nonselective black paint one-glass collector is best (number 8). The use of honeycomb (number 9) or anti-reflection glass with a selective surface (number 22) is only an added economic burden. It can be demonstrated that in cases of low wind condition it would be more cost effective to have no cover sheet for collectors which are to be used for pool heating.

Collectors which give comparable efficiencies at hot water conditions are collectors with nonselective black paint 1-glass (number 8), nonselective black paint 2 glass (numbers 1, 11 and 12), nonselective black paint 1-glass with honeycomb (number 9), nonselective black paint 2 glass with honeycomb (number 10), selective black chrome 2 glass (number 21) and selective black nickel 2 glass (number 5). The top performer is a black nickel with 2 anti-reflection glass (number 22). A best choice from this list would be a nonselective black 1-glass collector, however, because of cost and practicality. This particular collector was produced on contract for LeRC, and more test experience will be required to determine this collector's life and performance reliability.

When collectors are to be used for solar a/c, the temperature levels at which the collector is to operate ($\sim 200^{o}$ F) requires the use of selective surfaces (22, 21, 5), nonselective black surfaces with a honeycomb (numbers 9, 10), or a selective surface in a vacuum condition (number 16). Note the importance of basing collector performance on an all-day basis in the case of collector 16. One advantage of a selective surface in a vacuum is the inherent protection of the coating with such a system.

Considerations for coating protection have a special importance in the case of a black nickel coating due to potential degradation of this coating under humid, hot conditions. A coating which appears to have the potential for greater life than black nickel, gives about the same performance, and is now commercially available, is black chrome (number 21). The use of anti-reflection glass to increase solar transmission and a selective coating (number 22) clearly leads to an outstanding performer for the conditions of solar a/c. In the case of solar-Rankine requirements, Table VI demonstrates that collectors which are good performers at solar a/c conditions do well at solar Rankine temperature conditions.

The same good performers for solar a/c also show a good rating in the case of clear day winter heating (Table VI). However, in this case a nonselective black paint 2 glass collector performs very well (1, 11, 12, and 13). It would appear from Table VI that building systems requiring both heating and cooling would perform best with collectors that incorporate methods of reducing collector heat loss (selective surface, vacuum, honeycomb) and increasing the amount of transmitted solar energy (anti-reflection glass).

It is not expected that flat plate solar collectors will generally be very effective on a cloudy day. This is clear from the performance values given in Tables VI(a) and (b) for heating on a cloudy winter day. On such days, low heat loss types of collectors (number 16) are most effective.

Collector ranking based on cost effectiveness. - An interesting cost effectiveness study on different collector designs was made by Honeywell on contract to NASA (ref. 3), and those results are briefly reiterated here. In this study it was possible to assess the cost effect of design variations such as transparent cover type, number of covers and the type of coating

(nonselective vs selective). This cost effectiveness comparison was made possible by the use of a standard collector box design and performance testing with a duplicate of the simulator used at the Lewis Research Center. Table VII from reference 4 shows a cost effectiveness comparison of different design configurations with a baseline collector having a black nickel coating and two transparent glass covers. This comparison is for the limited mass production quantity of 100 000 ft^2/year.

It is clear from Table VII that for a/c and heating applications, there is a cost effectiveness advantage in using a collector with a selective coating (black nickel). The collector system of black nickel with one glass and one Tedlar transparent covers gives the highest value of relative cost effectiveness. The next best collector combination is black nickel with two covers of anti-reflection glass. A defect in the data of Table VII is that it does not take into account overall system performance. A system that includes an absorption air conditioner would probably be more cost effective with a black nickel - 2 anti-reflective glass collector than with a black nickel glass/Tedlar collector. This is due to the greater cooling obtainable from absorption a/c machines with collectors of high performance.

Collector Performance Degradation

The use of the solar simulator for measuring performance degradation is demonstrated by the results shown in figures 19(a) and (b). Performance correlations are presented in these two figures for a black paint - 2 glass - mylar honeycomb collector before and after a four month outdoor exposure, and for a black nickel 2 glass collector before and after a nine month outdoor exposure.*

---

*These collectors were placed in the NASA-Lewis outdoor facility described in reference 2.

In figure 19, performance degradation appears to be evident in both the collector heat loss (slope of correlation lines) and the coating absorptance (intercept of correlating lines). The major cause of performance degradation in the case of the black paint - 2 glass - mylar honeycomb appears to be a lowering in the coating absorptance. Although extensive testing for performance degradation has not been performed, the brief results presented here demonstrate the value of a standardized approach for gauging the performance as a function of life.

CONCLUSIONS

Use of a solar simulator for collector testing has been shown to be an effective tool for collector performance comparison and selection, and for performance prediction in "real life". The latter has been demonstrated by comparison of collector testing under both simulated and actual conditions.

Collector thermal efficiency data are reported here for a total of 23 collectors, including several different basic designs. These various designs encompass most of the important variables that can affect collector performance, including:

1. Selective surfaces for decreasing radiation loss.
2. Vacuum for decreasing or eliminating convection losses.
3. Honeycomb for reducing convection and radiation losses.
4. Anti-reflection glass for increasing the amount of transmitted solar energy.
5. Use of tube sheet material for a practical, low-cost absorber panel for efficient heat transfer.
6. Use of 1 or 2 transparent covers for reducing radiation and convection losses.
7. Use of plastics and glass for the transparent cover material.
8. Use of high absorptance coatings for increased collection efficiency.

Based on calculated all-day efficiency obtained from the solar simulator, it was possible to establish a performance ranking for pool heating,

hot water heating, solar a/c, solar Rankine systems, and solar heating. This performance ranking shows that the use of vacuum, selective surfaces, honeycomb, and anti-reflecting glass in collector designs has a definite performance advantage in buildings employing solar heating and cooling. Although the addition of these features increases cost, a preliminary assessment suggests that some of these high performing collectors may also be more cost effective, even though they do cost more.

An evaluation of collector performance by an inspection of collector performance parameters indicated that simply reducing collector heat loss does not always guarantee a good performing collector. The following are items that must be considered to insure a good collector design:

1. Coating absorptance and emittance.
2. Absorber plate heat transfer efficiency.
3. Sufficient insulation to reduce significant amounts of back and edge heat losses.
4. Transmittance of cover system.

A quantity which was also measured, and which may require additional consideration in some cases, is the collector heat capacity.

For completion of the collector selection process for any given application, more information would be needed on collector life and collector performance degradation rate, and overall reliability. Some test data were taken to illustrate how the simulator test approach can be used for measuring performance degradation due to exposure to outdoor operating conditions.

For any given application, the final collector selection will of course be determined from information on collector initial performance, performance degradation rate, cost, reliability, and life.

APPENDIX A

COLLECTOR HEAT CAPACITY

A heat balance on a collector which is undergoing transient heating or cooling may be written as follows:

$$Q_{in} = Q_u + Q_L + Q_{storage} \tag{A1}$$

The heat into the collector system may be expressed as

$$Q_{in} = AF'\alpha\tau q_{dr} \tag{A2}$$

The useful energy as

$$Q_u = AGC_p(T_0 - T_1) \tag{A3}$$

The heat loss as

$$Q_L = AF' U_L(\bar{T}_f - T_a) \tag{A4}$$

and the energy going into collector storage in terms of a collector heat capacity

$$Q_{storage} = AC_c \frac{d\bar{T}_f}{dt} \tag{A5}$$

Combining equations (A1) to (A4) and solving for the storage energy one obtains

$$C_c \frac{d\bar{T}_f}{dt} = F'[\alpha\tau q_{dr} - U_L(\bar{T}_f - T_a)] - GC_p(T_0 - T_1) \tag{A6}$$

The inlet and outlet temperatures may be written in terms of the average temperature of the collector fluid

$$T_0 - T_1 = (\bar{T}_f - T_1)/K \tag{A7}$$

where

$$K = \frac{G C_p}{F' U_L}\left(\frac{F'}{F_R} - 1\right)$$

The K factor derived in reference 6 is approximately equal to 1/2. From equation (A7) one obtains for a constant inlet temperature

$$\frac{d\bar{T}_f}{dt} = K \frac{dT_o}{dt} \tag{A8}$$

The standard heat capacity test is run by turning off the simulator lamps ($q_{dr} = 0$) at the condition where the inlet temperature equals to the ambient temperature ($T_1 = T_a$). Therefore, after substituting (A8) and (A7) into equation (A6) one obtains

$$C_c K \frac{dT_o}{dt} = -\left[F' U_L K (T_o - T_a) + G C_p (T_o - T_a)\right] \tag{A9}$$

rearranging and setting up the integration limits

$$C_c \int_{T_0(t_1)}^{T_0(t_2)} \frac{dT_o}{(T_o - T_a)} = -\int_{t_1}^{t_2} \left(F' U_L + \frac{G C_p}{K}\right) dt \tag{A10}$$

integrating and solving for the collector heat capacity.

$$C_c = \frac{\left(F'U_L + \frac{GC_p}{K}\right)(t_2 - t_1)}{\ln\left[\frac{T_0(t_1) - T_a}{T_0(t_2) - T_a}\right]} \qquad \text{(A11)}$$

APPENDIX B

TRANSIENT RESPONSE TIME - TIME CONSTANT

To understand how quickly a collector responds to changing conditions, equations (A1) to (A5) are combined and written in the following manner:

$$\int_0^t \frac{dt}{C_c} = \int_{\bar{T}_{f_1}}^{\bar{T}_{f_2}} \frac{d\bar{T}_f}{F'\left[\alpha\tau q_{dr} - U_L(\bar{T}_f - T_a) - \frac{GC_p(\bar{T}_f - T_1)}{K}\right]} \tag{B1}$$

integrating equation (B1) results in

$$\frac{t}{C_c}(F'U_L + 2GC_p) = \ln \left\{ \frac{F'\left[\alpha\tau q_{dr} - U_L\left(\bar{T}_{f_1} - T_a\right)\right] - \frac{GC_p\left(\bar{T}_{f_1} - T_1\right)}{K}}{F'\left[\alpha\tau q_{dr} - U_L\left(\bar{T}_{f_2} - T_a\right)\right] - \frac{GC_p\left(\bar{T}_{f_2} - T_1\right)}{K}} \right. \tag{B2}$$

Since $\bar{T}_f - T_1/K = T_0 - T_1$, the measured efficiency is defined as $\eta_{meas} = GC_p(T_0 - T_1)/q_{dr}$ and the calculated efficiency is defined as $\eta_{cal} = F'\left\{\alpha\tau \quad - \left[U_L(T_f - T_a)\right]/q_{dr}\right\}$.

Equation (B2) may be written as

$$\frac{\eta_{1,cal} - \eta_{1,meas}}{\eta_{2,cal} - \eta_{2,meas}} = e^{\frac{t\left(F'U_L + \frac{GC_p}{K}\right)}{C_c}} \tag{B3}$$

Since the calculated efficiency assumes equilibrium at time equal to zero when the collector has begun to receive the energy of the sun, the

following applies

$$\eta_{1,\text{cal}} \simeq \eta_{2,\text{cal}} \tag{B4}$$

$$\eta_{1,\text{meas}} = 0 \tag{B5}$$

The time constant will be defined as the time required for the actual efficiency to be 99 percent of the equilibrium efficiency or

$$\eta_{2,\text{meas}} = 0.99\ \eta_{2,\text{cal}} = 0.99\ \eta_{1,\text{cal}} \tag{B6}$$

Combining equations (B6) and (B3) and solving for the time constant

$$t_c = \left(\frac{C_c}{F'U_L + \frac{GC_p}{K}} \right) \ln 100 \tag{B7}$$

SYMBOLS

A_a	absorber area, ft^2
A'_e	effective collector area with shield, ft^2
A_e	effective collector area, ft^2
A_g	transparent cover area, ft^2
A_T	total collector area, ft^2
$\bar{a}_\theta$	performance correlation intercept for diffuse radiation, dimensionless
C_c	collector heat capacity, Btu/ft^2, ^oF
C_p	fluid heat capacity, Btu/lb, ^oF
F'	collector plate efficiency factor, dimensionless
F_R	collector plate heat-removal efficiency, dimensionless
G	flow rate of collector fluid, lb/hr-sq ft of absorber surface
K_{df}	ratio of diffuse to total radiation, dimensionless
K_{dr}	ratio of direct to total radiation, dimensionless
K_{FR}	flow factor modifier, dimensionless
K_{U_L}	heat loss modifier, dimensionless
$K_{\alpha\tau}$	incident angle modifier, dimensionless
q_{df}	incident diffuse solar radiation, $Btu/hr\text{-}ft^2$ (in collector plane)
q_{dr}	incident direct solar radiation, $Btu/hr\text{-}ft^2$ (in collector plane)
q_T	total solar radiation, $Btu/hr\text{-}ft^2$ (in collector plane)
T_a	ambient temperature, ^oF
$\bar{T}_f$	average collector fluid temperature, ^oF
T_o	fluid outlet temperature, ^oF
$\bar{T}_p$	average collector plate temperature, ^oF
T_1	fluid inlet temperature, ^oF

t	time, hr
U_L	overall collector heat loss coefficient, Btu/hr-ft^2, ^oF
α	collector surface absorptance, dimensionless
$\overline{\alpha\tau}$	$\alpha\tau$ product for diffuse radiation, dimensionless
ϵ	collector surface emittance, dimensionless
η	collector efficiency, dimensionless
τ	effective transmittance
θ_i	solar incident angle, degrees

Superscript:

–	average conditions

REFERENCES

1. F. F. Simon and P. Harlamert, Flat-Plate Collector Performance Evaluation. The Case for a Solar Simulation Approach. Paper presented at International Solar Energy Soc. Meeting, Cleveland, Oh. (1973).

2. R. W. Vernon, Solar Collector Performance Evaluated Outdoors at NASA-Lewis Research Center. Paper presented at NSF/RANN Workshop on Solar Collectors for Heating and Cooling Buildings, New York, N.Y. (1974).

3. J. W. Ramsey, J. T. Borzoni, and T. H. Holland, Development of Flat Plate Solar Collectors for the Heating and Cooling of Buildings. Honeywell, Inc. Rept 2852-40057; also NASA CR-134804 (1975).

4. K. Yass and H. B. Curtis, Low-Cost Air Mass 2 Solar Simulator. National Aeronautics and Space Adm. Tech Memo X-3059 (1973).

5. R. W. Vernon and F. F. Simon, Flat-Plate Collector Performance Determined Experimentally with a Solar Simulator. Paper presented at International Solar Energy Society, Annual Meeting, Fort Collins, Colo. (1974).

6. F. F. Simon, Comparison under a Simulated Sun of Two Black-Nickel-Coated Flat-Plate Solar Collectors with a Nonselective-Black-Paint-Coated Collector. TM X-3226.

7. F. F. Simon, Status of the NASA-Lewis Flat-Plate Collector Tests with a Solar Simulator. Paper presented at NSF/RANN Workshop on Solar Collectors for Heating and Cooling of Buildings. New York, N.Y. (1974).

8. F. F. Simon, Solar Collector Performance Evaluation with the NASA-Lewis Solar Simulator - Results for an All-Glass-Evacuated Tubular Selectively-Coated Collector with a Diffuse Reflector. National Aeronautics and Space Adm. Tech. Memo X-71695 (1975).

9. F. Simon, Standardized Solar Simulator Tests for Flat-Plate Solar Collectors. I: Soltex Collector with Two Transparent Covers. National Aeronautics and Space Adm. Tech Memo X-71338 (1975).

10. A. F. Souka and H. H. Safwat, Optimum Orientations for the Double-Exposure, Flat-Plate Collector and its Reflectors. Solar Energy, 10, 170 (1966).

11. F. F. Simon and E. H. Buyco, Outdoor Flat-Plate Collector Performance Prediction from Solar Simulator Test Data. AIAA 10th Thermal Physics Conference, Paper No. 75-741, Denver, Color. (1975).

12. A. M. Zarem, Introduction to the Utilization of Solar Energy. McGraw-Hill, New York (1963).

13. S. A. Klein, The Effects of Thermal Capacitance Upon the Performance of Flat-Plate Solar Collectors. M.S. Thesis, University of Wisconsin (1973).

14. R. W. Vernon, Status Report of Outdoor Solar Collector Tests At the NASA-Lewis Research Center. Paper presented at 1975 International Solar Energy Society Meeting, Los Angeles, California (1975).

TABLE I. - COLLECTORS TESTED

Number	Collector	Absorber material* and type	Collector area, A_T, sq ft	Cover area, A_g, sq ft	Absorber area, A_a, sq ft	Effective area, A_e, sq ft	Coating absorptance, α	Coating emittance, ϵ	Experimental constants			
									a_θ	b_θ	c_θ	b_o
1	LeRC black paint-2 glass	Cu (1)	16.3	15	13.8	13.8	0.97	0.97	0.75	0.833	0	-0.15
2	Barber CuO-1 glass	Cu (2)	8.6	6.9	6.9	6.9	.97	-----	.795	1.17	0	-.11
3	Barber CuO-1 glass, Al. honeycomb	Cu (2)	8.6	6.9	6.9	6.9	.97	-----	.795	1.17	0	-----
4	Beasely CuO-2 glass	Cu (2)	8.9	8	7.9	7.9	.86	.1	.59	.76	0	-.18
5	NASA/Honeywell black nickel-2 glass	Al (1)	16	15	13.5	13.5	.95	.07	.713	.504	0.14	-.16
6	MSFC black nickel-1 Tedlar	↓	7.9	7.4	6.1	5.7	.73	~.1	.567	.755	.141	-.11
7	MSFC black nickel-2 Tedlar	↓	7.9	7.4	6.1	5.7	.73	~.1	.533	.642	.0722	-.16
8	NASA/Honeywell black paint-1 glass	↓	16	15	13.5	13.5	.97	.97	.850	1.139	.161	-.078
9	NASA/Honeywell black paint-mylar honeycomb-1 glass	↓	↓	↓	↓	↓	↓	↓	.817	.806	.119	-.23
10	NASA/Honeywell black paint-mylar honeycomb-2 glass	↓	↓	↓	↓	↓	↓	↓	.735	.497	.284	-.20
11	NASA/Honeywell black paint-2 glass	↓	↓	↓	↓	↓	↓	↓	.728	.705	.251	-.15
12	Martin Marietta black paint-2 glass	↓	----	----	11.8	11.8	.996	.996	.748	.719	.197	↓
13	Trantor black paint-2 glass	Steel (4)	----	----	14.9	14.9	-----	-----	.701	.548	.601	↓
14	PPG black paint-2 glass	Al (1)	18.1	17.9	17.9	17.9	.95	.95	.615	.954	-.013	↓
15	Soltex CuO-1 glass-1 Lexan	Cu (2)	12	10.8	10	10	-----	-----	.574	.837	-.141	-.18
16	Owens-selective surface-glass-evacuated-tubular	Glass	14.4	21.6	17.4	17.4	.8	.09	.45	.24	0	+.43
17	ITC-selective surface-2 glass	Al (1)	27.9	24.8	23	22	~.9	~.3	.665	.648	-.0007	-.15
18	Solar Products black paint-1 glass	Cu (3)	12	9.6	10.5	9.3	-----	-----	.593	1.153	-.0861	-.078
19	Miromit black nickel-1 glass	Steel (2)	19.1	15.6	15.7	15.3	~.9	~.1	.689	.976	-.125	-.11
20	L.O.F. selective surface-2 glass	Steel (4)	6.3	5.5	5.3	5.3	-----	-----	.433	.718	-.175	-.15
21	NASA/Honeywell black chrome-2 glass	Steel (4)	16	15	13.3	13.3	.94	.07	.725	.687	-.050	-.17
22	NASA/Honeywell black nickel-2 AR glass	Al (1)	16	15	13.5	13.5	.95	.07	.85	.626	0	-.16
23	GE selective surface-2 Lexan	Al (1)	25.3	23.2	22.9	22.9	.95	.31	.673	.695	0	-.05

*Legend: 1. Tube sheet.
2. Tubes bonded to absorber plate.
3. Tubes clamped to absorber plate.
4. Spot welded absorber plate.

TABLE II. - NASA-LEWIS SOLAR SIMULATOR SUMMARY

Radiation source,
143 Lamps, 300 W each
GE-type ELH, tungsten-halogen dichroic coating
12^{o} Total divergence angle
Test area,
4 by 4 ft, maximum
Test condition limits,
Flux; 150 to 350 Btu/hr-ft^2
Flow; up to 1 gal/min (30 lb/hr-ft^2)
Inlet temp; 75^{o} to 210^{o} F
Wind; 0 to 10 mph at 75^{o} F

TABLE III. - COMPARISON OF SOLAR SIMULATOR AND AIR-MASS 2 PERFORMANCE

		Air-mass 2 sunlight	Simulator
Energy output, percent	Ultraviolet	2.7	0.3
	Visible	44.4	48.4
	Infrared	52.9	51.3
Energy uses	Absorptance (Selective surface)	0.90	0.90
	Glass transmittance	.85	.86
	Al mirror reflectance	.86	.88
	Solar cell efficiency, percent	12.6	13.4

TABLE IV. - COLLECTOR PERFORMANCE PARAMETERS

Collector	F'	F_R	$\bar{U}_L$, Btu/hr-ft^2, ^oF		$\alpha\tau$	α	ϵ
			Exp.	Theory			
LeRC-black paint-2 glass (1)	----	0.95	0.88	0.74	----	0.97	0.97
Beasley CuO, 2 glass (4)	----	.90	.85	----	----	.86	.1
NASA/Honeywell black nickel-2 glass (5)	0.96	.94	.56	.46	.74	.95	.07
MSFC black nickel-2 Tedlar (7)	.99	.95	.69	----	.56	.73	~.1
NASA/Honeywell black-1 glass (8)	.97	.90	1.3	----	.89	.97	.97
NASA/Honeywell black-2 glass-honeycomb (10)	.99	.96	.57	----	.77	.97	----
NASA/Honeywell black paint-2 glass (11)	.97	.93	.80	.74	.76	.97	.97
PPG (14)	.94	.85	1.1	----	.73	.95	.95
Owens (16)	----	----	.20	.15	.72	.8	.07

TABLE V. - EXPERIMENTAL COLLECTOR HEAT CAPACITY

Collector	Collector heat capacity, C_c, experimental	Collector heat capacity, C_c, estimated (ref. 13)	Time constant, (t_c), calculated min
Black nickel-2 glass (5)	0.54	0.5 - 0.6	9
MSFC 1 cover (6)	.48	.35 - .45	8
MSFC 2 cover (7)	.45	.5 - .6	8
Black paint-1 glass (8)	.45	.35 - .45	8
Black paint-honeycomb-2 glass (10)	.65	--------	11
Black paint-2 glass (11)	.61	.5 - .6	10
PPG (14)	.43	.5 - .6	11
Owens (16)	2.5	--------	72
ITT (17)	.71	.5 - .6	9

TABLE VI(a). - COLLECTOR PERFORMANCE RANKING - NOON HOUR PERFORMANCE BASIS

Clear summer day								Clear winter day		Cloudy winter day	
Pool heating		Hot water		Absorption a/c		Solar Rankine		Heating		Heating	
Collector number	η_{12}	Collector number	η_{12}	Collector number	η_{12}	Collector number	η_{12}	Collector number	η_{12}	Collector number	η_{12}
8	83.1	22	71.0	22	58.6	22	50.3	22	60.6	16	32.4
22	82.2	9	63.2	5	48.1	5	39.8	10	52.3	22	13.3
9	78.0	8	62.2	10	48.0	10	38.2	9	51.6	21	.11
2,3	77.3	10	60.9	9	45.9	21	36.1	5	49.9	5	.1
1	72.6	5	59.6	21	44.7	16	35.8	12	47.3	17	0
12	72.5	12	59.0	12	42.6	9	33.9	21	46.6	1	
10	70.7	21	57.8	1	41.1	17	31.4	1	45.8	2	
11	70.5	1	57.7	11	40.4	12,23	30.8	11	45.1	3	
21	69.9	11	57.1	17,23	40.0	1	30.1	8,13	43.7	4	
5	69.0	2,3,13	56.3	16	39.0	11	28.2	17	41.6	6	
13	68.0	23	53.8	13	38.9	13	24.9	23	40.9	7	
19	66.9	17	52.9	8	37.8	8	20.9	16	37.8	8	
2,3	66.3	19	49.9	2,3	33.1	19	20.3	2,3	34.9	9	
17	64.5	16	43.8	19	31.8	4	17.9	19	33.3	10	
14	59.3	4	43.0	4	27.9	2,3	17.6	4	29.7	11	
18	57.8	14	42.2	7	26.1	7	16.8	14	28.4	12	
4	56.6	6	41.1	15	25.4	15	15.9	7	27.6	13	
15,6	55.1	15	40.6	6	24.6	6	13.0	15	27.1	14	
7	51.5	7	39.7	14	23.4	14	10.9	6	26	15	
16	48.1	18	36.9	20	17.1	20	9.5	18	18.5	18	
20	41.8	20	29.5	18	13.1	18	0	20	18.1	19	
										20	

TABLE VI(b). - COLLECTOR PERFORMANCE RANKING - ALL DAY PERFORMANCE BASIS

Clear summer day								Clear winter day		Cloudy winter day	
Pool heating		Hot water		Absorption a/c		Solar Rankine		Heating		Heating	
Collector number	$\eta_{All-day}$	Collector number	$\eta_{All-day}$	Collector number	$\eta_{All-day}$	Collector number	$\eta_{All-day}$	Collector number	$\eta_{All-day}$	Collector number	$\eta_{All-day}$
8	77.4	22	60.0	22	44.7	22	35.8	22	50.7	16	26.2
22	76.1	5	49.8	16	39.3	16	34.8	10	41.9	22	15.7
2	71.1	9,10	49.7	5	35.5	5	26.6	5	40.5	5	7.5
9	69.7	8	49.1	10	34.1	21	23.7	9	39.6	21	6.4
12	66.8	12	47.6	21	32.4	10	23.2	16	37.7	10	6.2
1	66.6	21	47.4	9	30.6	17	19.8	21	37.1	17	3.8
11	64.9	16	46.5	23	29.2	23	19.7	12	36.5	23	3.3
10	64.5	1	46.3	12	28.9	9	18.8	1	35.6	1	3.0
21	64.1	11	45.8	17	28.6	12	17.2	11	34.2	9	2.5
5	63.9	23	45.3	1	28.0	1	17.1	17	32.7	12	1.9
23	63.1	13	45.0	11	26.7	11	15.2	23	32.5	11	1.1
13	62.7	2	43.7	13	24.4	13	12.0	13	32.4	15	.6
19	61.7	17	43.3	8	22.5	19	10.4	8	31.6	19	0
17	59.5	19	39.3	19	20.2	8	9.0	19	23.9	4,7	
14	53.6	4	33.3	2	19.2	4	8.8	2	23.8	2,6	
16	53.2	6	32.0	4	17.2	7	8.3	4	21.2	8	
18	53.0	14	31.8	7	16.3	15	7.8	7	19.8	13	
4	51.1	15,7	31.1	15	15.5	2	7.3	14	19.7	14	
6	50.7	18	26.6	6	14.2	6	5.3	15	19.1	18	
15	49.5	20	22.4	14	12.9	20	4.7	6	17.8	20	
7	46.9			20	9.9	14	4.2	20	12.4		
20	37.7			18	5.4	18	0	18	10.5		

TABLE VII - COST EFFECTIVENESS FOR VARIOUS COLLECTOR DESIGNS (REF. 3)

Configuration	Cost effectiveness		η,* percent
	Steel	Aluminum	
Baseline (black nickel - 2 glass)	1.00	1.00	44.5
Black nickel - 1 glass	1.03	1.01	41.5
- glass/Tedlar	1.13	1.11	46.5
- 1 Lexan	.92	.92	41.5
- 2 AR glass	1.03	1.06	55.0
Non-selective - 2 glass	.80	.93	33.0
- 1 glass	.72	.83	26.5
- glass/Tedlar	.79	.91	30.0
- 1 Lexan	.55	.64	23.0
- 2 AR glass	.85	.99	42.5
Black chrome - 2 glass	.93	.93	42.0

* At 250 Btu/hr-ft^2 and $\Delta T = 120^{\circ}$ F.

$$\text{Cost Effectiveness} = \frac{\left(\frac{\text{Cost/Area}}{\eta}\right)_{\text{Baseline}}}{\left(\frac{\text{Cost/Area}}{\eta}\right)_{\text{Alternate Configuration}}}$$

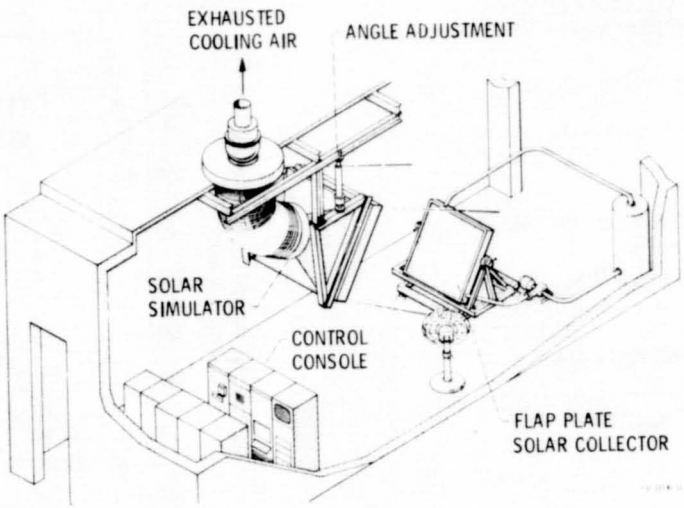

Figure 1. - Indoor test facility.

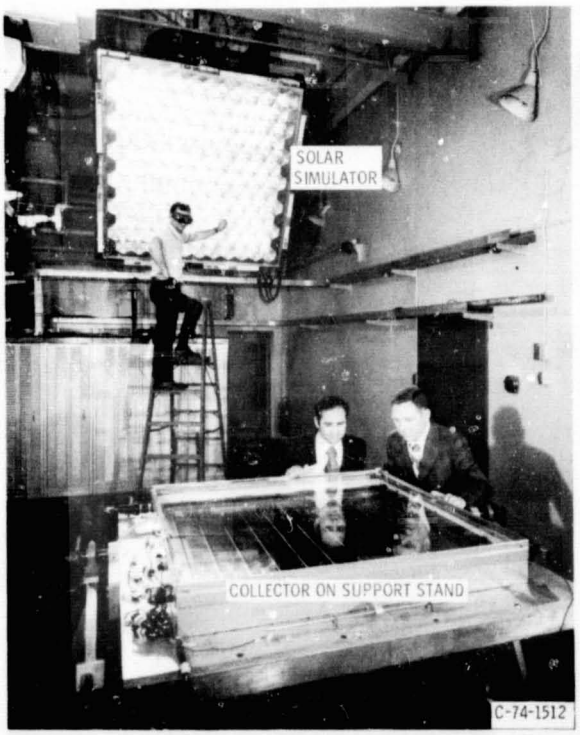

Figure 2. - Indoor facility used to experimentally determine solar collector performance.

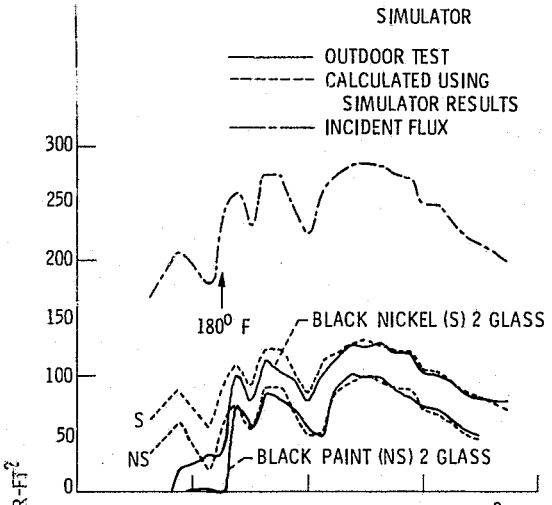

(c) WIND VELOCITY, 3-7 MPH; T_{AMB} AT 12:00, 45° F.

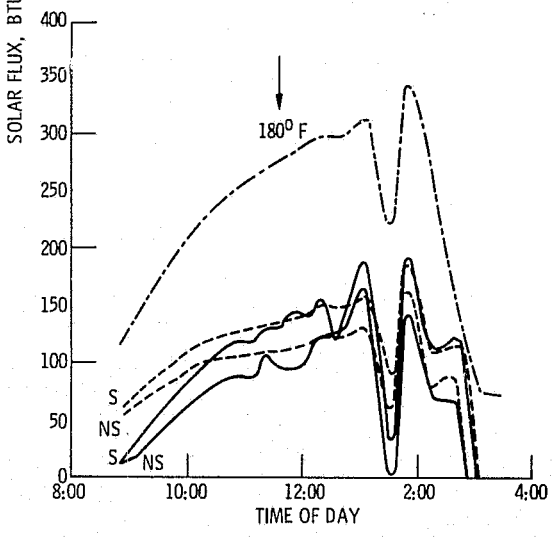

(d) WIND VELOCITY, 3-8 MPH; T_{AMB} AT 12:00, 63° F.

Figure 3. - Concluded.

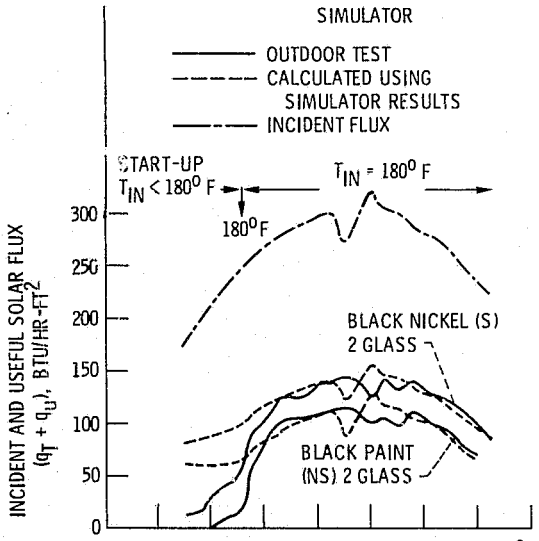

(a) WIND VELOCITY, 5-10 MPH; T_{AMB} AT 12:00, 50° F.

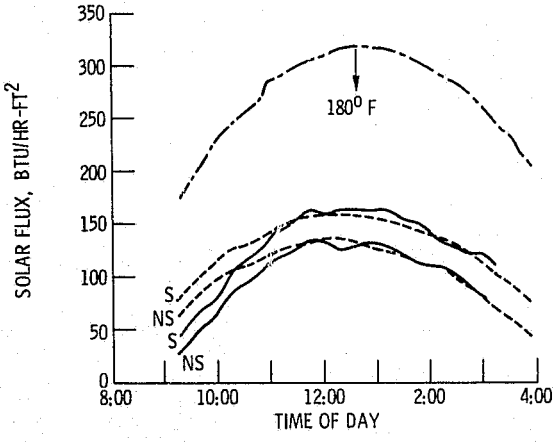

(b) WIND VELOCITY, 5-10 MPH; T_{AMB} AT 12:00, 50° F.

Figure 3. - Outdoor versus indoor (simulator) collector tests.

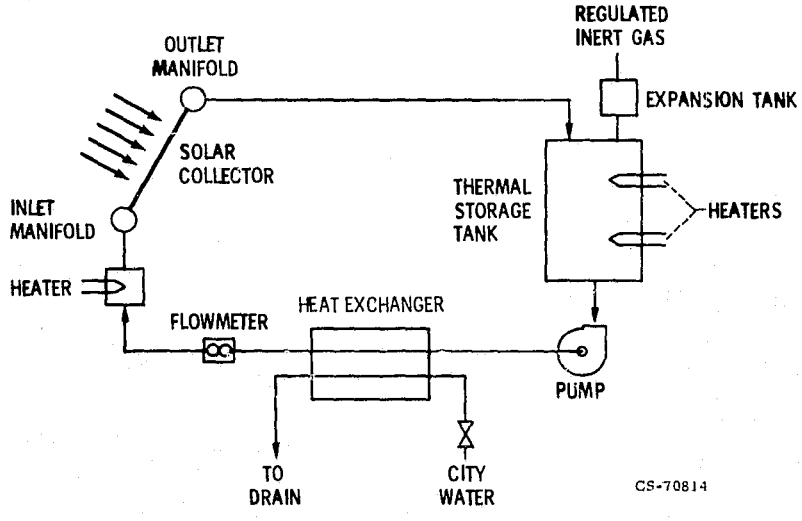

Figure 4. - Schematic of liquid flow loop.

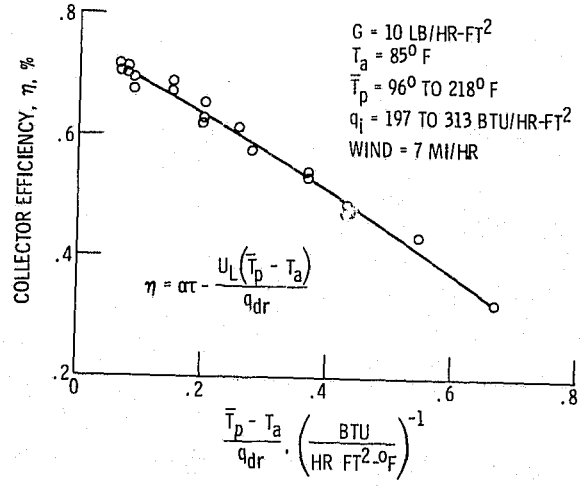

(a) NASA/HONEYWELL BLACK Ni 2 GLASS.

Figure 5. - Collector performance correlation.

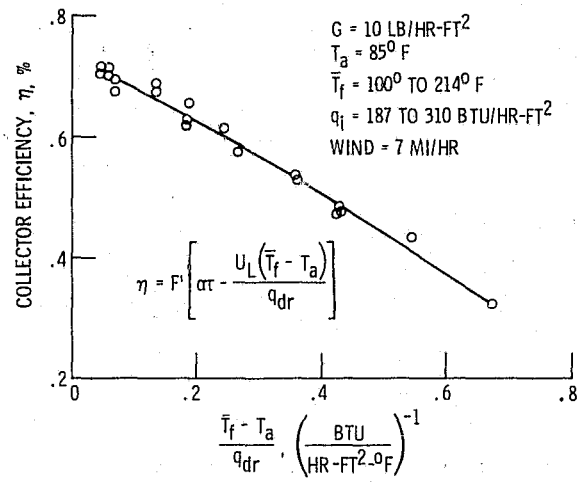

(b) NASA/HONEYWELL BLACK Ni 2 GLASS.

Figure 5. - Continued.

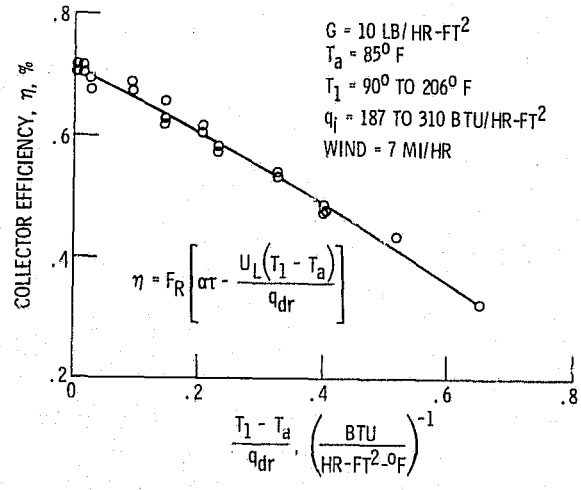

(c) NASA/HONEYWELL BLACK Ni 2 GLASS.

Figure 5. - Concluded.

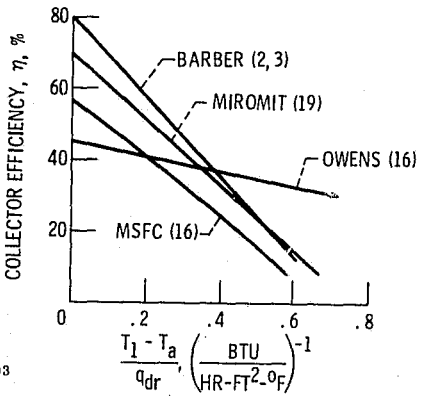

CS-74193

Figure 6. - Zero incidence performance curves for selective surface - one cover collectors.

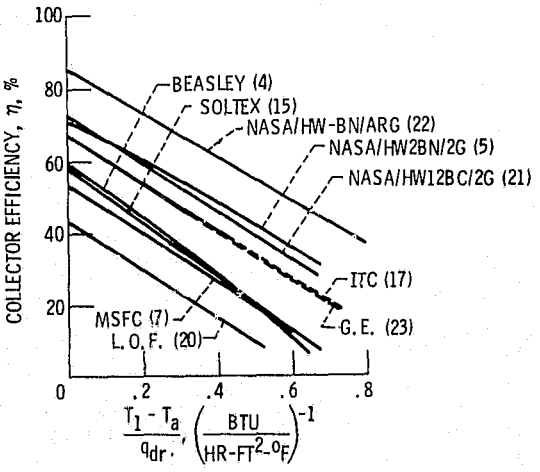

CS-74196

Figure 7. - Zero incidence performance curves for selective surface two cover collectors.

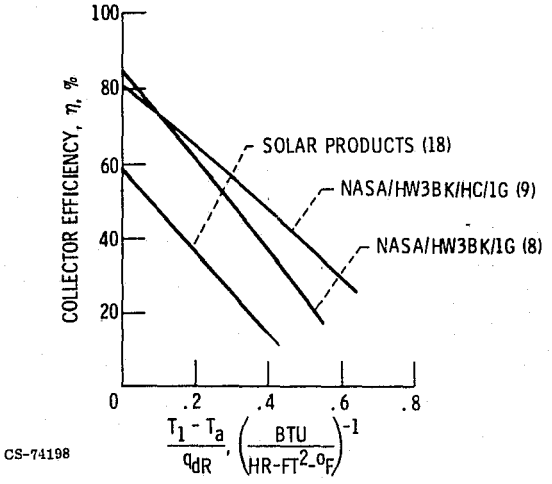

Figure 8. - Zero incidence performance curves for nonselective surface one cover collectors.

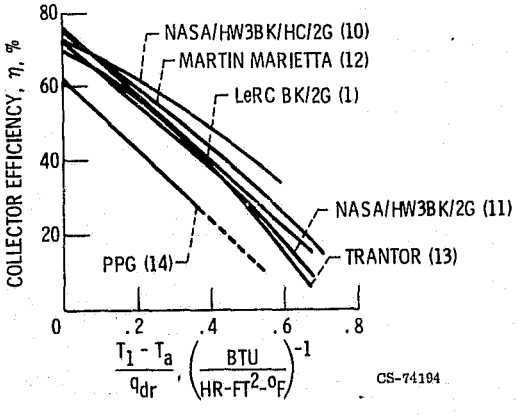

Figure 9. - Zero incidence performance curves for nonselective surface two cover collectors.

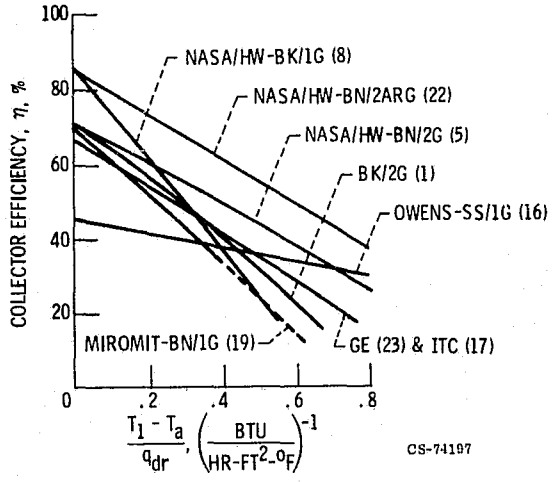

Figure 10. - Some comparisons of different collector types.

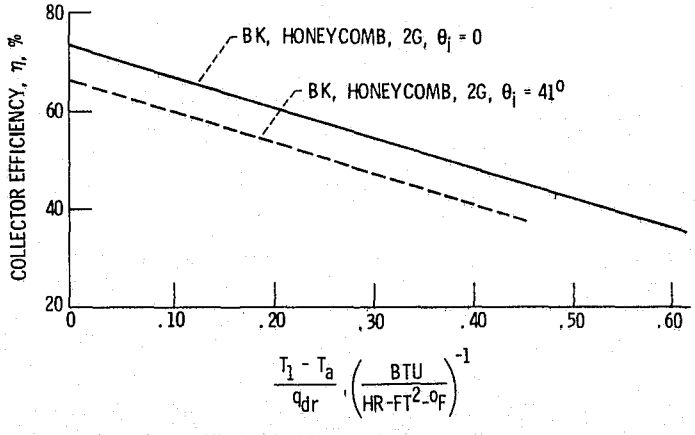

Figure 11. - Effect of incident angle (θ_i) on collector performance.

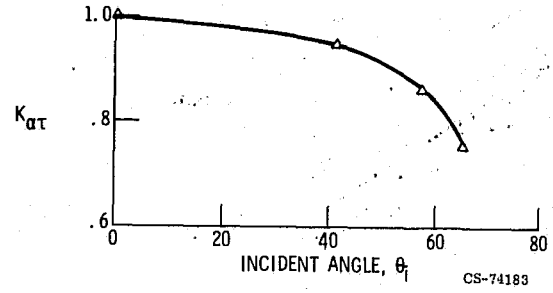

Figure 12. - Incident angle modifier for a black-nickel 2 glass collector (5).

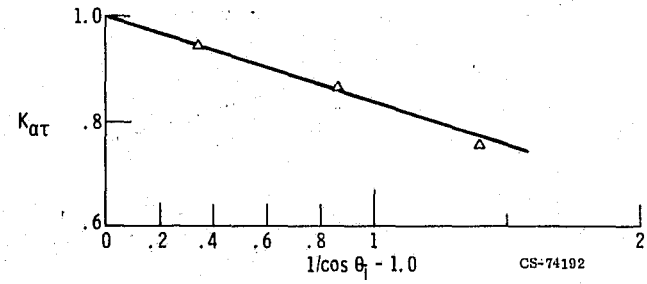

Figure 13. - Correlation of incident angle modifier for a black-nickel 2 glass collector (5).

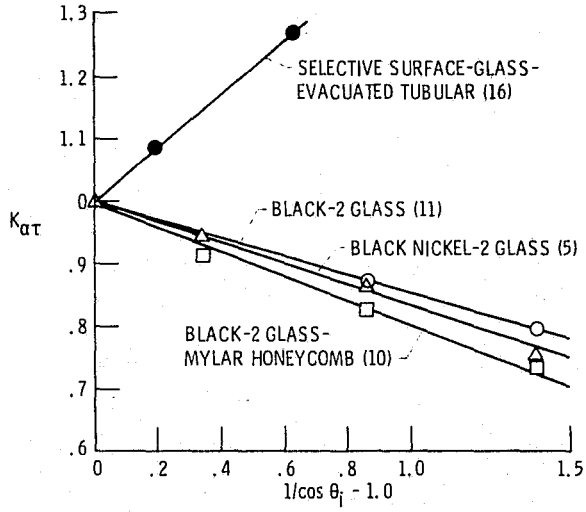

Figure 14. - Correlation of incident angle modifier.

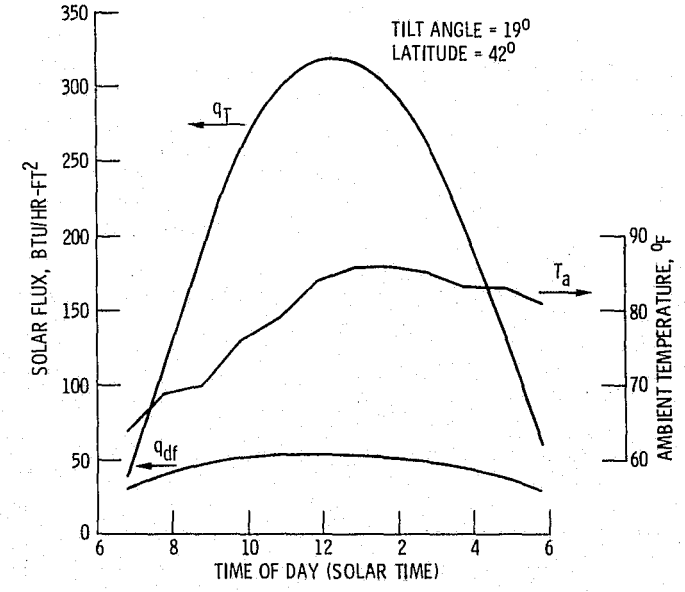

Figure 15. - Clear summer day solar data.

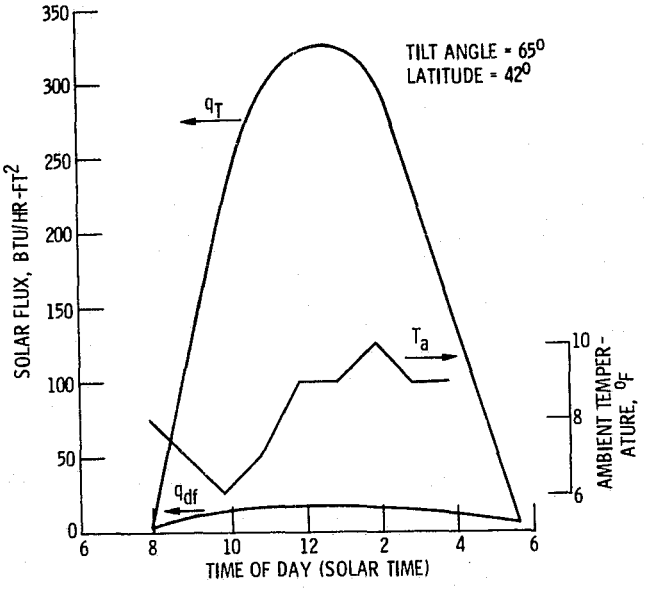

Figure 16. - Clear winter day solar data.

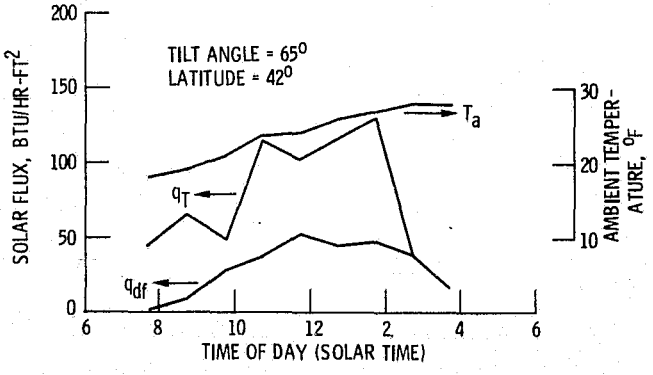

Figure 17. - Cloudy winter day solar data.

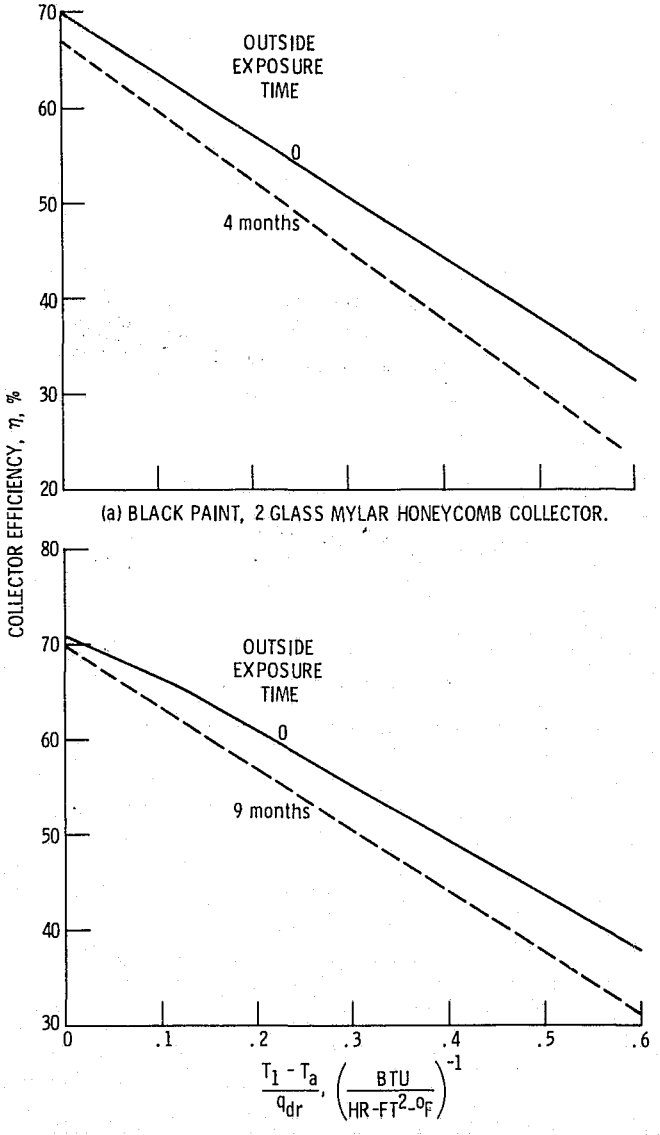

(a) BLACK PAINT, 2 GLASS MYLAR HONEYCOMB COLLECTOR.

(b) BLACK-NICKEL, 2 GLASS COLLECTOR (5).

Figure 19. - Outdoor performance degradation.

E-6293

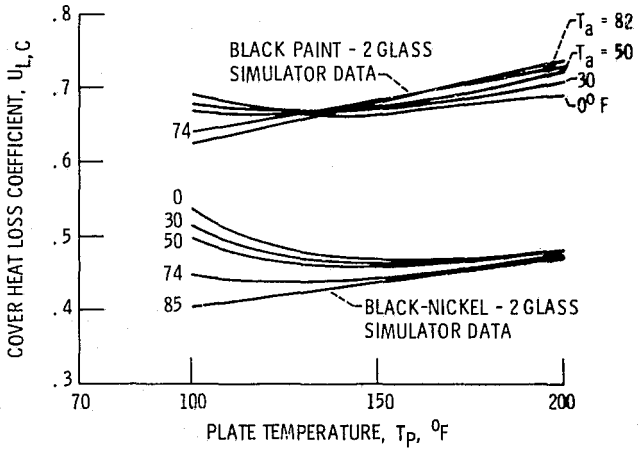

Figure 18. - Effect of ambient temperature on heat loss coefficient. (Ref. 11)